International Journal of Concrete Structures and Materials

RESEARCH Open Access

Experimental and Theoretical Investigations on the Bond–Slip Behavior of Newly Poured Concrete and Reinforcement Bars Under Traffic-Induced Vibrations in Bridge Widening

Yan Qiao[1], Weihua Zhang[2], Jinsheng Cheng[3], Lei Tong[3], Chuanzhi Sun[1*], Jibing Deng[4] and Fuhe Ge[5]

Abstract

This study investigates the bond–slip behavior of newly poured concrete and reinforcement bars under traffic-induced vibrations in bridge widening. Center pull-out tests were conducted on C60 concrete specimens with HTRB400 steel bars to examine the effects of bar diameter, vibration frequency, amplitude, and anchorage length. Based on the experimental data, the bond–slip constitutive model of newly poured concrete-reinforcement bars was developed. Test results indicated that larger bar diameters reduced ultimate bond stress and relative slip. Specimens with 8 *d* (*d* is the diameter of reinforcement bar) anchorage length exhibited lower bond strength than those with 5 *d*. Vibration amplitude had minimal influence on bond behavior, while higher frequencies decreased bond stress but increased slip. The constitutive model can provide a reliable prediction of bond behavior under dynamic disturbances. The findings offer practical insights for bridge widening projects, ensuring structural integrity under traffic loads.

Keywords Travelling disturbance, Bond–slip behavior, Reinforced concrete, Constitutive model

1 Introduction

Reinforced concrete structures are widely used in modern construction due to their high stability, excellent durability, relatively simple production process, and cost-effectiveness. With advancements in construction technology, significant improvements have been made in both the materials (e.g., reinforcement types, concrete compositions, and admixtures) and structural forms of reinforced concrete, solidifying its status as one of the most prevalent construction materials today (Deng et al., 2023; Ming et al., 2021; Zhou et al., 2022).

However, cast-in-place concrete is susceptible to various environmental disturbances, such as traffic-induced vibrations, which can damage its internal microstructure and degrade its mechanical properties. Most old bridges undergo widening under semi-open traffic conditions. During such expansion projects, the newly poured concrete in the widening sections cannot fully cure in a short time. As a result, the vibration waves generated by passing vehicles-particularly the dynamic coupling effects of axles-inevitably affect the bonding and slip behavior

*Correspondence:
Chuanzhi Sun
schzh_xzh@163.com
[1] School of Civil Engineering and Architecture, Suqian College, Suqian 223800, China
[2] China Power Engineering Consultant Group Zhongnan Electric Power Design Institute Co., Ltd, Changsha 410000, China
[3] Suqian City Urban Construction Investment (Group) Co., Ltd, Suqian 223800, China
[4] China Construction Fifth Engineering Bureau Co., Ltd, Changsha 410004, China
[5] Central Southern China Electric Power Design Institute Co., Ltd. of China Power Engineering Consulting Group, Wuhan 430061, China

between the freshly poured concrete and reinforcing steel.

The bonding action between reinforcement and concrete depends mainly on the chemical adhesion, friction and mechanical occlusion, and the anchorage at the ends of the reinforcement (Feng et al., 2025; Xu et al., 2023). The generation of internal bond in reinforced concrete members varies at different stress stages due to factors such as the surface form of the reinforcement and the loading method. Bonding performance, as an important factor to ensure the stability of reinforced concrete structure, is easily received by the concrete strength grade, the thickness of the protective layer of concrete, the surface form of reinforcing steel, the anchorage length, hoops and other factors (Darwin et al., 1992, 1996; Orangun et al., 1977). At present, most of bond–slip performance tests of reinforced concrete are under static loading. Solomos et al. (Solomos & Berra, 2010) found that the failure modes of reinforced concrete components vary greatly with and without confinement in practical engineering. Under unconstrained action, most of the reinforced concrete specimens mainly underwent splitting failure. Under constrained action, most of the specimens performed pull-out failure. As the load rate increased, the ultimate bonding stress of reinforced concrete increased. Yan (Yan, 1992), Mo and Chan (Mo & Chan, 1996) investigated the effect of different loading rates on the bond properties between light round reinforcement and concrete. It was concluded that the loading rate had little effect on the bond strength of the reinforcement and concrete, but the slip corresponding to the ultimate bond stress of the reinforcement and concrete increased as the loading rate increased. Kayyali (Kayyali & Yeomans, 1995) carried out bending damage tests on reinforced concrete beams and investigated the effect of different ribbed reinforcement surface coating materials on bond–slip performance of reinforced concrete. The results showed that the specimens coated with epoxy resin reinforcement had the best bonding performance compared with the specimens reinforced with galvanized reinforcement and ordinary reinforcement. The existing research has conducted in-depth research on settlement, shrinkage and creep of new bridges.

During the construction process of bridge widening projects, due to the requirement of uninterrupted traffic, the vibration caused by vehicle loads throughout the entire process of concrete solidification and hardening of the bridge affects the strength growth of newly poured concrete at the wet joint. The performance of the interface between new and old concrete have received little attention. However, there are relatively few studies on the bond–slip performance of reinforced concrete under traveling disturbances.

The reinforced concrete bond–slip constitutive models are studied under static loading (Guizani et al., 2017; Lin et al., 2019; Wu & Zhao, 2013), but the reinforced concrete bond–slip constitutive model under dynamic loading has not yet had a clear expression. The bond stress–slip model was obtained by Leroy (Leroy & Gergely, 1967) in 1967 based on the center pull-out test of reinforcement bars with a specially designed single rib. The bond stress was explicitly related to the position of the loading end in the bond–slip relationship equation proposed by Mirza and Houde (Saeed & Houde, 1979) in 1979. In 1997, Kankam (Charles, 1997) obtained the bond stress–slip relationship for glossy, cold-finished and hot-rolled bars based on the test results of two-end tensile specimens. The scholars of the above early studies used a single expression to represent the bond–slip constitutive model. At the same slip, the bond strength obtained by the scholars varied greatly, and the maximum slip corresponding to the peak bond strength of the bond ontology were also different. In addition, the bond strength corresponding to the same slip also varied greatly. The bond–slip constitutive relationship is an important index for the accuracy of the detailed analysis of structure members. A large number of experimental and theoretical studies on it have been carried out. Eligehausen et al. proposed local bond stress–slip relationships of deformed bars under generalized excitations (Eligehausen et al., 1983). The bond–slip constitutive relationship studied by Haraji (Haraji & Mabsout, 2002) can consider the slip to cleavage stage as a smooth straight line. In the rising segment, the bond–slip constitutive relationship is described in Eq. (1). In the residual segment, the bond–slip constitutive relationship is described in Eq. (2):

$$\tau = \tau_{\mathrm{u}}\left(\frac{s}{s_{\mathrm{u}}}\right)^{0.3}, \tag{1}$$

$$\tau = 0.35\tau_{\mathrm{u}}, \tag{2}$$

where s_{u} is the slip corresponding to the ultimate bond stress τ_{u}.

Li et al. (Gao, 2003) further investigated the bond–slip performance of high-performance concrete (concrete strength grade was C50) and derived the following bond–slip constitutive relationship equations:

$$\tau = \tau_{\mathrm{u}}\left(\frac{s}{s_1}\right)^{0.3} \quad 0 \le s \le s_1, \tag{3}$$

$$\tau = \tau_2 + \left(\frac{\tau_{\mathrm{u}} - \tau_2}{15 - s_1}\right)(15 - s) \;\; s_1 < s \le 15, \tag{4}$$

$$\tau = \tau_2 \ \ s > s_2, \tag{5}$$

where s_1 is the slip corresponding to the progression from the slip phase to the cleavage phase;s_2 and τ_2 are the slip and bond stress during the development from the splitting stage to the falling stage, respectively.

With the rapid development of modern cities, the contradiction between urban infrastructure and the rapidly growing transportation demand remains prominent. Widening of existing roads and bridges is an important way to meet the surge in traffic demand. In the actual construction, interrupt traffic is often applied to widening of existing roads and bridges. As a result, the bridge vibration caused by traveling loads will be transferred to the reinforced concrete of the spliced wide wet joints, which will have an impact on the bonding performance between the newly placed reinforcement and the newly poured concrete. In this article, the effects of reinforcement diameters, anchorage lengths, vibration frequencies and vibration amplitudes on the bond–slip performance of reinforced concrete specimens under traveling disturbance were investigated experimentally. Based on the results of reinforced concrete center pull-out tests, the bond–slip constitutive model of new-to-old reinforced concrete under traveling disturbance was proposed.

2 Experimental Program

2.1 Determination of Disturbance Parameters Caused by Traveling Loads

To truly and accurately study the effect of traffic disturbance on the performance of concrete using for bridge widening wet joints, this article relies on the bridge widening project of Lin'an to Jiande section of Linjin Expressway. Due to the uninterrupted traffic, the traffic flow has a greater impact on the determination of the disturbance parameters. When testing the disturbance parameters caused by traveling loads, the initial period of the test was selected as the full time period in the morning. Base on the field tests, it was found that the transmission and collection of vibration signals were more obvious when the traffic flow was larger, and the vibration signals were less obvious when the traffic flow was smaller. Therefore, in the afternoon, a time with high traffic flow was selected for measurement. A dynamic test system was used to determine the bridge vibration parameters caused by traveling loads. The test system mainly consisted of a vibration picker, a signal amplifier, a signal collector and a vibration test and analysis system. The vibration signal of the bridge vibration was converted into an analog signal by the vibration picker, which was amplified by the signal amplifier and transmitted to the signal collector. The signal acquisition instrument took the amplified analog signals for data acquisition and converted the analog signals into digital signals through the A/D conversion module. Sampling parameters were collected and controlled by a signal collector and a field monitoring computer. Various bridge dynamic data collected in the field were analyzed by dynamic test analysis and modal analysis software for bridge vibration test analysis and bridge vibration modal analysis. The vibration parameters were measured without interrupting the traffic. There were differences in the traffic flow in different time periods. The traffic load made the bridge produce different degrees of forced vibration, so the dynamic response of the bridge was measured to analyze, and ultimately get the vertical vibration amplitude and vibration frequency of the bridge caused by the traffic load. The instrumentation used for the test was the INV3062W collector and the Model 941B pickup as shown in Fig. 1. The 941B type pickup vibration exciter was a multi-functional machine, through the pickup micro-toggle switch, can directly measure the vertical acceleration. It was connected to a signal amplifier and can measure the vertical displacement of the bridge

(a) INV3062W collector (b) Model 941B pickup

Fig. 1 Data acquisition equipment

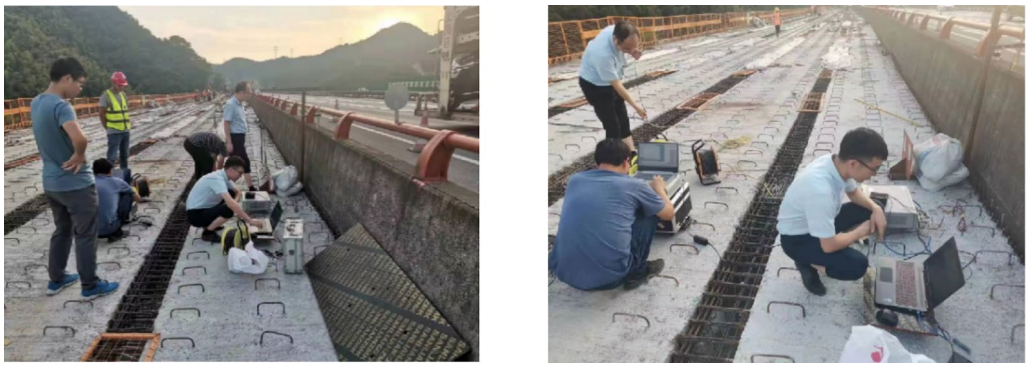

Fig. 2 Field data measurement

Table 1 Parameter design for specimens in the center pull-out tests

No.	*d* (mm)	l_0 (mm)	*A* (mm)	*f* (Hz)
D14i3j4d5	14	70 (5*d*)	3	4
D14i3j4d8	14	112 (8*d*)	3	4
D16i1j4d5	16	80 (5*d*)	1	4
D16i2j4d5	16	80 (5*d*)	2	4
D16i3j4d5	16	80 (5*d*)	3	4
D16i3j4d8	16	128 (8*d*)	3	4
D16i3j3d5	16	80 (5*d*)	3	3
D16i3j2d5	16	80 (5*d*)	3	2
D18i3j4d5	18	90 (5*d*)	3	4
D16i0j0d5	16	80 (5*d*)	0	0

d is the diameter of the steel bar; l_0 is the anchorage length of the steel bar; *A* is the vibration amplitude; *f* is the vibration frequency

under forced vibration. Six measurement points were distributed at 1/4 and 1/8 points on both ends of the bridge, as well as 5 points in the middle of the bridge, for a total of 30 measurement points. On site testing is shown in Fig. 2. The test results indicated that the vibration frequency caused by traveling disturbance measured at the project site was 2–4 Hz, and the vibration amplitude was 1–3 mm.

2.2 Test Specimen Design

The vibration duration of all the specimens was selected from the vibration to the initial set stage (3 h) for the test. According to the measured disturbance parameters caused by traveling loads, the reinforced concrete bond–slip performance test under traveling disturbance was conducted using the center pull-out tests, with the vibration frequency (2 Hz, 3 Hz, 4 Hz), vibration amplitude (1 mm, 2 mm, 3 mm), rebar diameter (14 mm, 16 mm, 18 mm), and anchorage length (5 *d*, 8 *d*) as the main variables. The specimen parameters were set, as shown in Table 1. D denotes the bar diameter, i denotes the vibration amplitude, j denotes the vibration frequency, and d denotes the anchorage length. D14i3j4d5, for example, refers to the specimen with a bar diameter of 14 mm, subjected to simulated vibration with a vibration amplitude of 3 mm and a vibration frequency of 4 Hz, and with an anchorage length of 5 times the diameter of the steel bar. The concrete of the specimens were the same as the C60 concrete used in the actual bridge widening construction. The mix ratio of the C60 concrete is shown in Table 2. The specimens were made of HRB400 steel bars used in the actual bridge widening construction. The property parameters of the steel bars are listed in Table 3.

2.3 Test Specimen Production

Concrete specimens were produced according to the standard in GB/T 50152-2012 (National standards of People's Republic of China, 2012). Each specimen was a standard cubic with a side length of 150 mm. Before the specimen production, the steel bar was processed and

Table 3 Performance parameters of HRB400 steel bars

Steel bars	*d* (mm)	Yield strength (MPa)	Ultimate Strength (MPa)
HRB400	14	415	580
HRB400	16	546	725
HRB400	18	690	865

Table 2 Mix ratio of C60 concrete

Cement	Sand	Stone	Water	Fly ash	Slag	Water reducer
340kg/m^3	698kg/m^3	1100kg/m^3	152kg/m^3	60kg/m^3	90kg/m^3	4.8kg/m^3

milled in half along the length direction. Then, a slot was cut at the center of the milled steel bar, with a width of 4 mm and a height of 2 mm. The anchoring section of the steel bar was polished flat and cleaned with acetone; and then strain gauges were pasted at the bottom of the slot in each bonding section of the steel bar with 502 adhesive. Three strain gauges were arranged in the anchored section, one was pasted at the center of the anchored section and the other two were pasted at each both ends along the center of the anchored section. The distance between each strain gage was 1.25*d*, and the specific arrangement is shown in Fig. 3. The main performance parameters of the resistance strain gauges are listed in Table 4. A layer of film was first covered on the strain gauges. The strain gauges were pasted and the slots were filled with adhesive. Then, steel wires were used to fix both ends of the steel bar. The adhesive was removed after it dried completely. Finally, spot welding was done to fix both sides of the steel bar.

Table 4 Performance parameters of strain gauges

Model number	Resistance value (Ω)	Sensitivity factor	Grid length × grid width (mm × mm)
BX120-3AA	120 ± 0.2%	2.05 ± 0.28%	3 mm × 2 mm

Fig. 3 Design drawing of test specimens (unit: mm)

A removable concrete test mold with a size of 150 mm × 150 mm × 150 mm was used. Holes were drilled in the center of both sides of the mold according to the different diameters of the steel bars. Medical bandages were wrapped around the unbonded section at the free and loaded ends of the reinforcement. Then, a layer of black waterproof tape was wrapped around the outside of the bandages, after which the corresponding polyvinyl chloride (PVC) casing was put on, and an appropriate amount of epoxy resin was filled with cotton and sealed between the PVC casing and the holes of the black tape. A layer of lubricant was applied to the inside of the test specimen mold to facilitate demolding. The reinforcement bars with PVC sleeves were mounted on the removable test molds. The test specimens are prepared as shown in Fig. 4. Firstly, sand, stone, fly ash, slag, water, water reducer were weighted for prepare the test specimens. Secondly, sand, cement, fly ash, slag and other fine dry materials and coarse aggregates were poured into the mixer for dry mixing for 2 min, and after dry mixing, water mixed with water-reducing agent was repeatedly and uniformly poured back and forth from left to right, and stirred for 2 min. Thirdly, the formed concrete was poured into the pre-prepared molds, inserted and placed on the vibrating table to vibrate until no air bubbles overflowed. Fourthly, the smoothed specimen was bolted to the vertical vibration test bench. The electromagnetic vertical vibration test bench (Fig. 5) is used to simulate traveling disturbance with a vibration frequency of 4 Hz and an amplitude of 3 mm. After vibration, the specimen was cured for one day. Finally, the specimen mold was removed and the specimen was placed in a standard concrete curing box for 28 days.

2.4 Test Setup and Loading Scheme

The test setup is shown in Fig. 6(a). A homemade reaction frame was fixed to the upper part of the hydraulic

Fig. 5 Vertical vibration test bench

(a) Cutting slots in steel bars

(b) Pasting strain gauges

(c) Sealing steel bars

(d) Sleeve into mold

(e) Perturbing

(f) Demolding

Fig. 4 Specimen preparation process

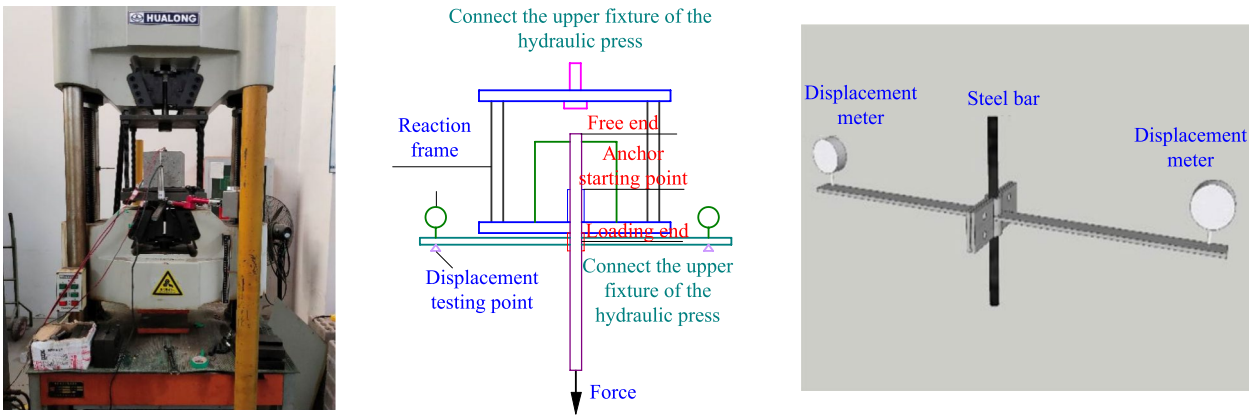

(a) Specimen in testing (b) Specimen connection (c) Displacement measuring device

Fig. 6 Test setup

testing machine with connectors. The specimen was placed at the bottom of the reaction frame. The steel bars at the lower part of the specimen were clamped with fixtures in the lower crossbeam of the hydraulic testing machine. The self-made displacement testing device was installed between the specimen and the crossbeam, with the displacement meter pressed against both ends of the device. The wiring between the displacement gauge and strain gauge was connected to the TMR-7300 tester. The connection joint was wrapped with insulating tape. The displacement loading mode was used in the test. In order to make the measured slip value more accurate, a smaller loading speed of 0.2 mm/min was selected. The load was collected by computer. The strain of strain gauges inside the reinforcement and the synchronized displacement of the bond–slip specimens were collected by the TMR-7300 acquisition system. The collection frequencies were 5 Hz.

The average bond stress of reinforced concrete specimens was calculated as:

$$\tau = \frac{F}{\pi d l_0}, \tag{6}$$

where F was the tensile force on the reinforcement (N).

The specimens were connected as shown in Fig. 6(b). The slip of the reinforcement and concrete was averaged from the values measured by the displacement gauge at the loading end (Lu et al., 2011). Displacement measurement at the loading end was performed using the homemade device as shown in Fig. 6(c). The displacement meter was placed against the two ends of the device beam after being fixed to the lower part of the test specimen reinforcement with a bolt connection.

The data measured by the displacement meter were the rough slip of the anchored section of reinforcement and concrete, and the deformation of the BC section of the reinforcement in the drawing process should also be taken into account. The average slip of the reinforcement and concrete specimen was:

$$S_u = \frac{1}{2}(S_1 + S_2) \tag{7}$$

The internal shape variable of the reinforcement was:

$$\Delta S_l = \frac{F}{E_s A_s} L_{BC}, \tag{8}$$

where E_s was the modulus of elasticity of the rebar (provided by the rebar manufacturer); As was the cross-sectional area of the reinforcement (mm^2); L_{BC} was the distance between points B and C (mm).

The actual slip of the reinforcement and concrete was:

$$s = S_u - \Delta S_l \tag{9}$$

At this stage, the experimental studies on bond–slip properties of reinforced concrete are usually based on the center pull-out test, while the calculated average bond stress were taken as the actual bond stress.

3 Results and Discussion

3.1 Test Phenomena and Failure Modes

Three distinct failure modes were identified in the center pull-out tests conducted on reinforced concrete specimens subjected to both static loads and traveling disturbances, as detailed in Table 5 and illustrated in Fig. 7.

Figure 7(a) depicts the pull-out damage observed in a specimen under static loading conditions. When the specimen was damage, there was no obvious crack on the surface of the specimen. At the beginning of loading, the

Table 5 Failure modes of specimens under static loads and traveling disturbance

Specimen no.	Failure mode	Specimen no.	Failure mode
D16i0j0d5	Rebar was pull-out	D14i3j4d5	Rebar was pulling off
D14i3j4d8	Rebar was pulling off	D16i1j4d5	Splitting damage
D16i2j4d5	Splitting damage	D16i3j4d5	Splitting damage
D16i3j4d8	Splitting damage	D16i3j3d5	Splitting damage
D16i3j2d5	Splitting damage	D18i3j4d5	Splitting damage
D16i0j0d5	Splitting damage	D14i3j4d5	Splitting damage

slip between the free end and the fixed end of the reinforcement was zero; with the increase of load, the slip between the reinforcement and the concrete gradually occurred, and after the peak load was reached, the reinforcement was pulled out, and thus the bond anchorage between the reinforcement and the concrete was destroyed. From the damage mechanism, it was known that reinforced concrete was subjected to chemical adhesive forces in the initial stage; with the increase of the load, the slip increased with it, and the friction and mechanical occlusion forces came into play; when the peak load was reached, the reinforcement was pulled out, and there was still a part of the residual force.

Under traveling disturbance, the splitting damage of the specimens with a diameter of 16 mm and 18 mm was observed, as shown in Fig. 7(b). When the specimen damaged, the cracks in the specimen surface developed rapidly, instantaneous splitting, and accompanied by a large acoustic noise. From the damage mechanism can be known that the occurrence of splitting damage chemical adhesive force, friction and mechanical occlusal force had played a role, but mainly to mechanical occlusal force was dominant; with the increase of the load, the concrete was subjected to the formation of the circumferential tensile stresses of the ribbed reinforcement, when the load continued to increase until it exceeded the tensile strength of the concrete, the concrete internal penetration of the cracks was generated from the inside out [54]. After reaching the peak load, the specimen cracked instantaneously.

Under traveling disturbance, the rebar pull-off damage of the specimens with a diameter of 14 mm was observed, as shown in Fig. 7(c). When the specimen was damaged, the rebar was pulled off, and there were no obvious cracks in the surface of the specimen, and a large acoustic noise was produced. It can be known from the damage mechanism, the rebar was pulled off in the process of chemical adhesion, friction and mechanical occlusion force had played a role, and the three and the concrete between the force generated by more than the ultimate tensile strength of the rebar, resulting in the rebar was pulled off and the concrete did not have a significant impact. After being disturbed, the bond between the reinforcement and the concrete exceeded the ultimate tensile strength of the reinforcement, and the reinforcement was destroyed before the peak bond stress was reached.

From the above three failure modes, it can be found that the specimens in the static state were pull-out damage and the ultimate bond stress was small. While the specimens under low-frequency disturbance were mainly splitting damage, and the ultimate bond stress was significantly increased compared with that of the specimens in the static state. It indicated that the appropriate disturbance enhances the bonding performance between the reinforcement bars and the concrete.

(a) Rebar was pull-out (b) Splitting damage (c) Rebar was pull-out

Fig. 7 Failure mode

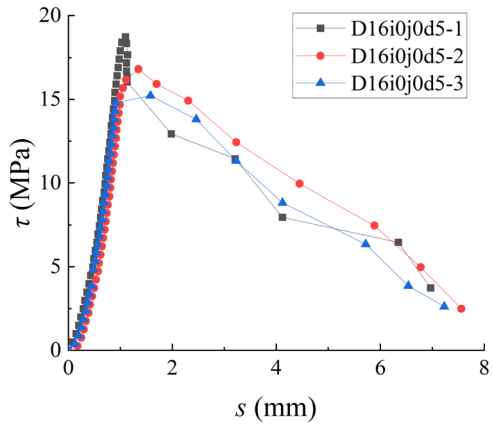

(a) D16i0j0d5

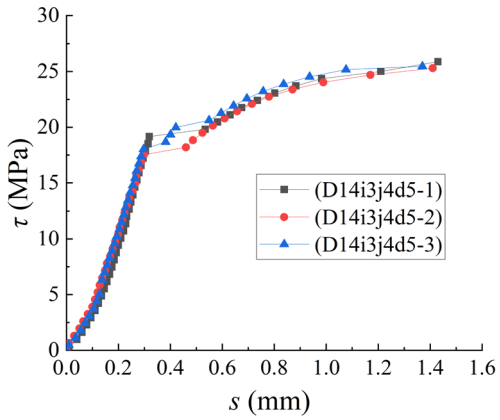

(b) D14i3j4d5

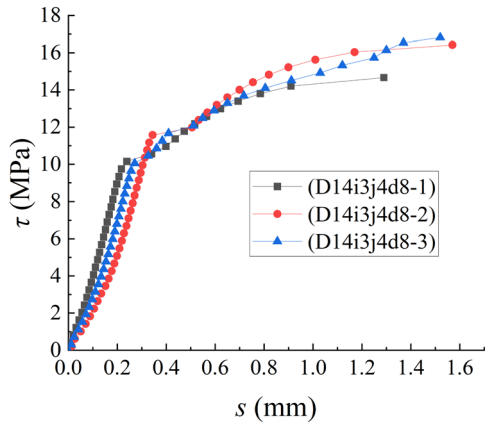

(c) D14i3j4d8

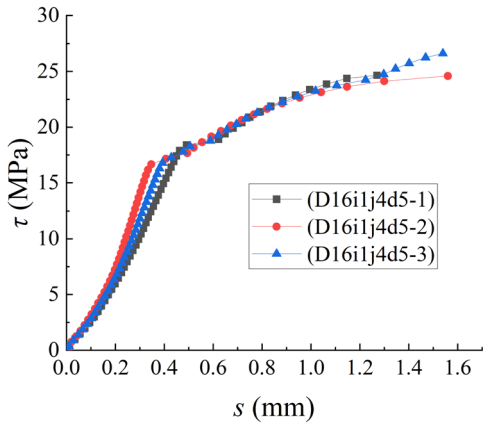

(d) D16i1j4d5

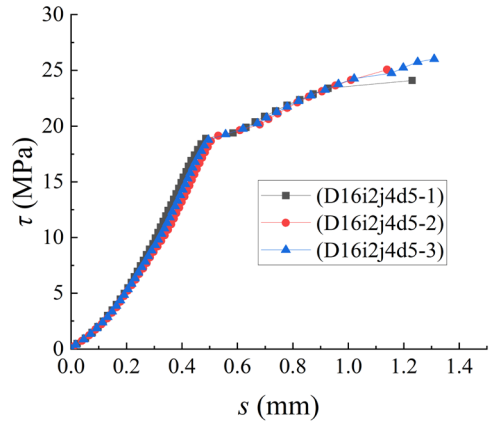

(e) D16i2j4d5

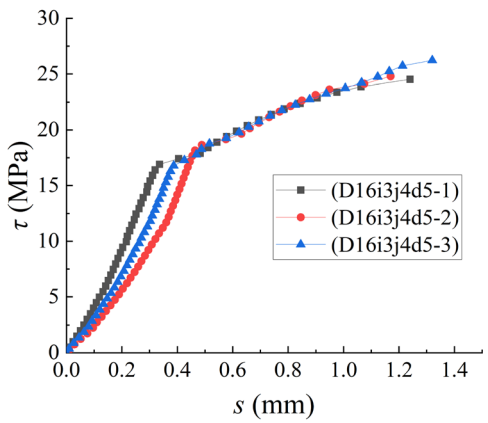

(f) D16i3j4d5

Fig. 8 Bond–slip curves of specimens under each working condition

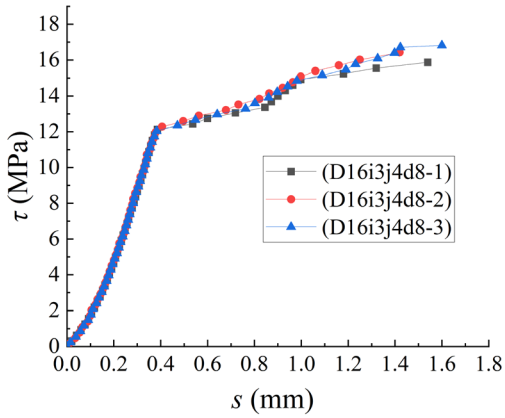

(g) D16i3j4d8

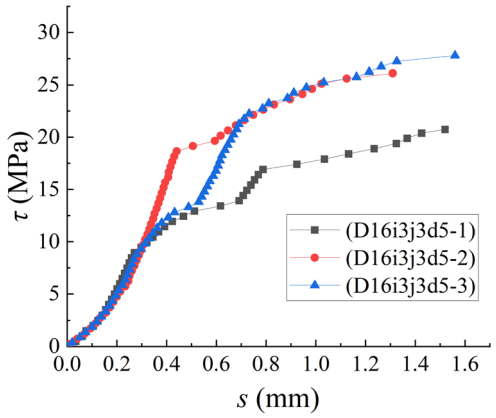

(h) D16i3j3d5

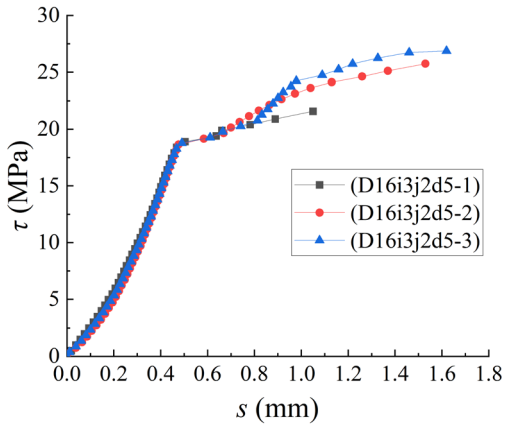

(i) D16i3j2d5

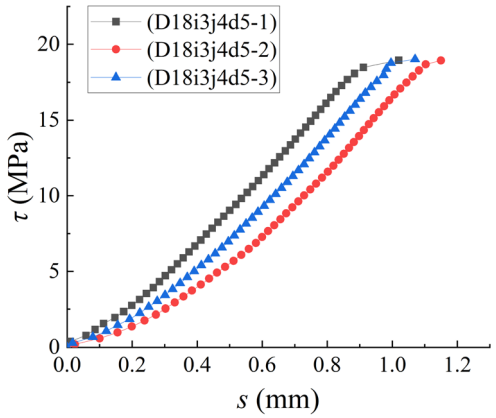

(j) D18i3j4d5

Fig. 8 continued

Table 6 Average of the test result of the specimen under travelling disturbance

Specimen no.	F_{cr} (kN)	F_u (kN)	S_u (mm)	τ_u(MPa)
D16i0j0d5	56.47	67.82	1.55	16.87
D14i3j4d5	66.77	78.66	1.40	25.56
D14i3j4d8	66.86	78.66	1.43	15.97
D16i1j4d5	92.25	101.68	1.46	25.29
D16i2j4d5	91.07	100.72	1.23	25.05
D16i3j4d5	91.52	101.28	1.24	25.19
D16i3j4d8	96.21	105.31	1.52	16.37
D16i3j3d5	89.65	100.04	1.30	24.88
D16i3j2d5	90.06	99.42	1.40	24.72
D18i3j4d5	88.21	96.48	1.08	18.96

Note: F_{cr} (kN) is the cracking load of the specimen; F_u (kN) is the ultimate load of the specimen; τ_u (MPa) is the ultimate bond stress between concrete and reinforcement; S_u (mm) is the ultimate slip between concrete and reinforcement

3.2 Bond–Slip Curves

The bond–slip curves of the specimens are shown in Fig. 8. Table 6 summarizes the center pull-out test results of the specimens under static state and traveling disturbance. The bond–slip curves of the specimens under each working condition mainly presented two curve forms, the first one was the full curve form (extraction damage specimen in the static state), its curve can be divided into slip, cleavage, descent, residual four stages, with the increasing amount of slip the curve continues to rise, and after reaching the ultimate stress, it slowly declined to the stabilization; the second one was the curve of the only rising section (cleavage damage and reinforcement pulling off the damage) was divided into slip, cleavage stage, with the increasing amount of slip the curve raise continuously, and after reaching the ultimate stress it suddenly ruptured with

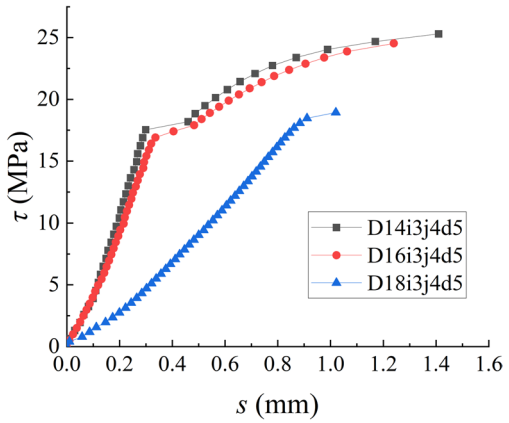

Fig. 9 Bond–slip curves for the specimens with different bar diameters

Table 7 Summary of bond–slip behavior for specimens with different rebar diameters

Diameter (mm)	Ultimate bond stress reduction	Ultimate slip reduction	Failure mode
14	— (baseline)	— (baseline)	Rebar was pulling off
16	3% vs 14mm	12%	Splitting damage
18	25% vs 14mm	28%	Splitting damage

no subsequent descending section of the curve. It can also be seen that before the ultimate stress was reached and the amount of slip was very small (slip stage), whether it was the full curve or only the rising section of the curve, the curves of specimens under the same working condition were almost overlapped and the curves were almost straight, so it can be concluded that at this point of time, the bond stress and the amount of slip were increasing in a more or less linear manner; the curve of the splitting stage was much more gentle compared with that of the slip stage, and it was a kind of parabola development.

3.3 Effect Factors on Bond Properties of Reinforced Concrete Under Traffic Vibration

3.3.1 Effect of Reinforcement Diameter

Figure 9 shows the bond–slip curves for the specimens with different bar diameters. Summary of bond–slip behavior for different rebar diameters is listed in Table 7. The increase in the diameter of the reinforcement made the reduction of the thickness of the cover concrete more prone to damage, which reduced the bond stress, and the larger the diameter of the contact surface between the reinforcement and the concrete was also larger, the greater the mechanical occlusion force between the cross ribs of the reinforcement and the concrete, which reduced the amount of relative slippage between the reinforcement and the concrete.

3.3.2 Effect of Anchorage Length

Figure 10 shows the bond–slip curves for the specimens with different anchorage lengths. Summary of bond–slip behavior for different anchorage lengths is listed in Table 8. It was found that the longer the anchorage length, the more uneven the distribution of bond stress, the average bond strength of the specimen at the time of damage and the actual maximum bond strength differ greatly, and the bond strength decreased with the increase of the anchorage length.

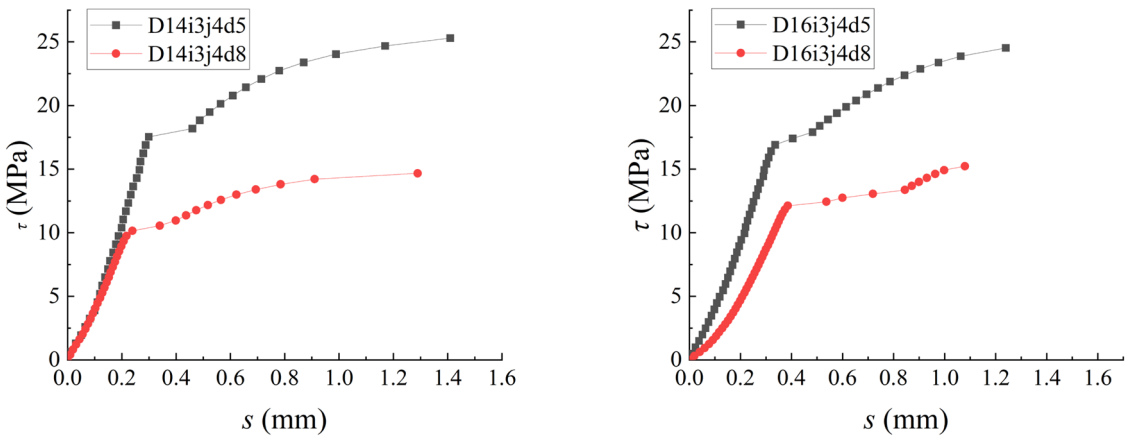

(a) Specimens with bar diameters of 14 mm (b) Specimens with bar diameters of 16 mm

Fig. 10 Bond–slip curves of the specimens with different anchorage lengths

Table 8 Summary of bond–slip behavior for specimens with different anchorage lengths

Diameter (mm)	Anchorage length	Curve trend	Ultimate bond stress reduction	Ultimate slip reduction	Failure mode
14	5 *d*	Linear → parabolic	— (baseline)	— (baseline)	Rebar was pulling off
16	8 *d*	Linear → parabolic	42% vs 5d	9%	Splitting damage
18	8 *d*	Linear → parabolic	↓35% vs 5d	13%	Splitting damage

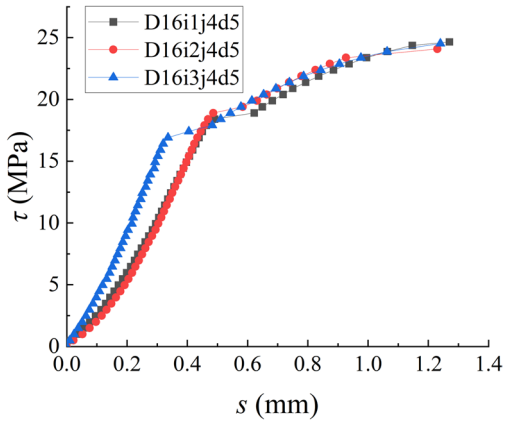

Fig. 11 Bond–slip curves for different vibration amplitudes

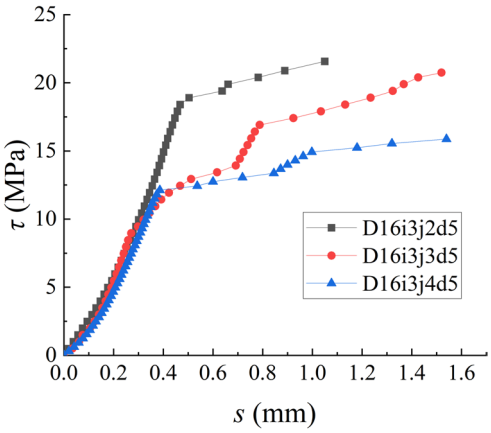

Fig. 12 Bond–slip curves for different vibration frequencies

3.3.3 Effect of Vibration Amplitude

Figure 11 shows the bond–slip curves of the specimens at different vibration amplitudes. The trend of the bond–slip curve of the specimen with a bar diameter of 16 mm was basically the same when subjected to different vibration amplitudes, which was almost linear growth of the slip and bond stress in the initial stage and then grew in an irregular curve. At the early stage of slip, the bond stress of the specimen at a vibration amplitude of 3 mm was the greatest and the curves were basically the same for the specimen with vibration amplitudes of 1 mm and 2 mm. At the middle and late stages of slip, the bond stresses were basically the same for the specimen with vibration amplitude of 1 mm, 2 mm and 3 mm. The slips of the specimens at different vibration amplitudes were not much different. Therefore, the influence of different vibration amplitudes on the ultimate stress, ultimate slip and the trend of bond–slip curve of the specimen was not obvious.

3.3.4 Effect of Vibration Frequency

Figure 12 shows the bond–slip curves of the specimens at different vibration frequencies. The trends of the bond–slip curves of the specimens at vibration frequencies of 2 Hz, 3 Hz and 4 Hz were basically the same. In initial stage of the slip, the three curves were almost linear growth and basically overlapped before the parabolic-like curve growth. The bond stress was decreased with the increase of the vibration frequency. Compared with the specimen at a vibration frequency of 2 Hz, the bond stresses of the specimens at vibration frequencies of 3 Hz and 4 Hz were decreased by about 4% and 26%, respectively. The relative slip was increased with the increase of the vibration frequency. Compared with the specimen at a vibration frequency of 2 Hz, the relative slip of the specimens at vibration frequencies of 3 Hz and 4 Hz were increased by about 45% and 46%, respectively. An increase in vibration frequency implies that the specimen is subjected to more vibration cycles per unit time, resulting in more frequent stress cycles within the material. These frequent stress cycles accelerate the accumulation of fatigue damage within the material, facilitating the initiation and propagation of micro-cracks. Consequently, as the vibration frequency increases, the interior of the specimen sustains greater damage. This heightened damage level contributes to a reduction in the ultimate bond stress of the specimen, which corresponds to an increase in the relative slip between the components.

3.3.5 Influence of Traveling Disturbance

Figure 13 shows the bond–slip curves of the specimens in static state and traveling disturbance. The bond–slip curve of the specimen in the static state was a full curve with ascending and descending segments. The specimen

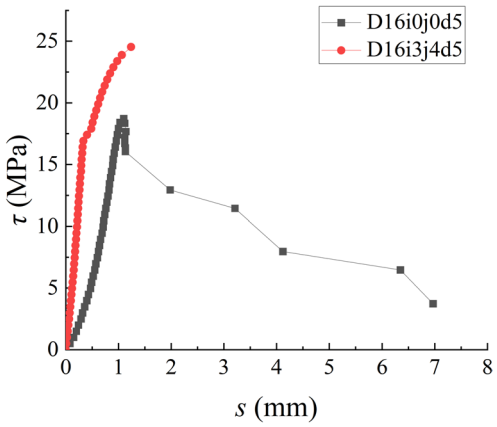

Fig. 13 Bond–slip curves in different states

under traveling disturbance had only ascending segments. Compared with the specimen under traveling disturbance, the ultimate bond stress of the specimen in the static state was decreased by about 40%. The failure mode of the specimens in the static state was pull-out damage, in which the reinforcement bar was completely pulled out, and thus the slip between the reinforcement bar and the concrete was greatly increased. The cohesion between reinforcement and concrete of the disturbed specimen was increased, and the reinforcement was difficult to be pulled out, and the bond strength of reinforcement and concrete was significantly improved.

It is important to clarify that the apparent increase in bond strength observed under moving disturbances can be attributed to changes in failure modes and the reinforcement of interfacial interactions, rather than an inherent or direct augmentation of the bond strength itself. In the context of concrete curing, the introduction of moderate disturbances can potentially foster greater material homogeneity and enhance the bonding at the interfacial level between the reinforcement and the concrete matrix. However, it is crucial to recognize that excessive or improperly timed disturbances during the curing process may have a detrimental effect, leading to a reduction in bond strength. Therefore, while controlled disturbances might offer benefits, they must be carefully managed to avoid compromising the structural integrity of the reinforced concrete.

3.3.6 Practical Guidelines for Bridge Widening

In bridge widening construction practices, systematic optimization of anchorage and seismic design should be implemented. Priority should be given to selecting 14 mm to 16 mm reinforcement bars to balance bond stress and slip demands. Specifically, 16 mm reinforcement bars exhibit only a 3% reduction in bond stress and a 12% decrease in slip, demonstrating superior overall performance compared to 18 mm reinforcement bars, which show a 25% reduction in bond stress and a 28% decrease in slip.

The anchorage length should be dynamically adjusted based on the bar diameter. Generally, 5 times the diameter of the reinforcement bar is taken as the most appropriate anchorage length. However, for larger diameter bars (especially those larger than 18 mm), the anchorage length should be increased by 15%–20% compared to smaller bars, and additional hooks or mechanical anchorage heads should be incorporated to address stress concentration risks induced by traffic disturbances.

The thickness of the concrete cover should increase with the bar diameter (e.g., at least 35 mm for 14 mm bars, 40 mm for 16 mm bars, and 50 mm for 18 mm bars). High-ductility concrete or interface bonding agents should be used to prevent splitting failure.

In seismic design, smaller diameter bars (especially those smaller than 18 mm) are suitable for high energy dissipation zones (such as plastic hinge regions in bridge piers) to leverage their larger slip for enhanced energy dissipation. Larger diameter bars, on the other hand, require compensation for insufficient energy dissipation through composite reinforcement or the addition of dampers. Construction techniques should emphasize the precision of reinforcement positioning and the compactness of concrete vibration. The curing period should be extended to 28 days to improve bond strength.

Quality inspection should focus on monitoring the bond strength and slip variations in the anchorage zones of larger diameter bars. Dynamic early warning can be achieved through embedded sensors, enabling a systematic approach to ensure the safety and durability of bridge widening projects in complex traffic environments, especially considering the effects of traffic-induced disturbances such as dynamic loads, fatigue damage accumulation, and stress concentration. This comprehensive strategy addresses the challenges posed by traffic disturbances and enhances the overall performance of the widened bridge structures.

4 Bond–Slip Constitutive Model of Reinforced Concrete Under Travelling Disturbance

Based on the commonly used ordinary reinforced concrete bond–slip constitutive models (Leroy & Gergely, 1967; Lin et al., 2019), it can be found that the form of the curve of the rising section is basically similar, and the correction coefficient α is different. The following relationship was adopted to carry out the study of reinforced concrete bond–slip constitutive relationship under the traveling disturbance:

$$\tau = \tau_{\mathrm{u}}\left(\frac{s}{s_{\mathrm{u}}}\right)^{\alpha}, \tag{10}$$

where τ_u is the ultimate bond stress; s_{u} is the ultimate slip corresponding to the ultimate bond stress; α is the correction factor of the curve.

Combined with the experimental data, the correction factor α is calculated in Table 9. For the specimens with bar diameters of 14 mm and 16 mm, α was calculated to be 0.40 after averaging, and α was taken to be 1.0 for specimens with a bar diameter of 18 mm. Substituting the correction factor α into Eq. (10), the theoretical bond–slip curve was obtained. Then, the theoretical bond–slip curve was compared with the experimental bond–slip curve, as shown in Fig. 14.

When comparing the test values with the theoretical values, it was found that when α was taken as 0.40, the test values of all disturbed specimens with bar diameters of 14 mm and 16 mm converged with the theoretical values in the curve splitting stage, and the fitting degree was poorer in the curve sliding stage. The experimental values of the specimens with a bar diameter of 18 mm converged with the theoretical values when α was taken as 1.0. Therefore, the degree of coupling between the data and the curve was reacted by calculating the coefficient R^2 of determination, and

Table 9 Calculation of correction factor *α*

Specimen no.	Ultimate bonding stress τ_{u} (MPa)	Maximum slip s_{u} (mm)	Correction factor α
D14i3j4d5-1	25.30	1.41	0.39
D14i3j4d5-2	25.47	1.37	0.42
D14i3j4d5-3	25.89	1.43	0.38
D14i3j4d8-1	14.67	1.19	0.32
D14i3j4d8-2	16.42	1.57	0.43
D14i3j4d8-3	16.81	1.54	0.41
D16i1j4d5-1	24.59	1.56	0.46
D16i1j4d5-2	25.65	1.27	0.32
D16i1j4d5-3	26.61	1.54	0.40
D16i2j4d5-1	25.05	1.14	0.36
D16i2j4d5-2	26.07	1.31	0.46
D16i2j4d5-3	24.08	1.23	0.43
D16i3j4d5-1	26.23	1.32	0.34
D16i3j4d5-2	24.80	1.17	0.36
D16i3j4d5-3	24.53	1.24	0.38
D16i3j4d8-1	15.87	1.54	0.41
D16i3j4d8-2	16.42	1.42	0.35
D16i3j4d8-3	16.82	1.60	0.38
D16i3j3d5-1	26.10	1.31	0.36
D16i3j3d5-2	20.74	1.02	0.40
D16i3j3d5-3	27.79	1.30	0.41
D16i3j2d5-1	25.74	1.53	0.41
D16i3j2d5-2	26.87	1.62	0.36
D16i3j2d5-3	21.57	1.05	0.41
D18i3j4d5-1	18.94	1.02	0.43
D18i3j4d5-2	19.00	1.07	0.96
D18i3j4d5-3	18.93	1.15	0.98

$$R^2 = 1 - \frac{\sum_{\mathrm{i}=1}^{\mathrm{n}} \left(\hat{y}_{\mathrm{i}} - \bar{y}_i\right)^2}{\sum_{\mathrm{i}=1}^{\mathrm{n}} \left(y_{\mathrm{i}} - \bar{y}_i\right)^2}, \tag{11}$$

where y_i is the bond stress value obtained by fitting the experimental data to the constitutive model, and $\bar{y}_i$ is its average value; $\hat{y}_{\mathrm{i}}$ is the bond stress measured in the experiment. The closer R^2 tended to 1 indicated that the bond–slip constitutive model fitted the experimental results better. R^2 of the bond–slip constitutive model fitting curves using Eq. (11) was calculated, as listed in Table 10.

From Table 10, it can be seen that the specimens with bar diameters of 14 mm and 16 mm were poorly fitted to the model curves when α was taken as 0.40. Observing the curve trend of all specimens, it was found that it was basically linear at the curve slip stage, so the linear expression for the curve slip stage was proposed on the basis of Eq. (10):

$$\frac{\tau}{\tau_{\mathrm{u}}} = \beta\left(\frac{s}{s_{\mathrm{u}}}\right) \tag{12}$$

The linear coefficient β was calculated by combining the experimental data of slip phase, as shown in Table 11. It can be seen that β was 2.0 after calculating the mean value for the specimens with bar diameters of 14 mm and 16 mm. The calculated values of the linear expression for the slip phase and the calculated values of the exponential expression for the splitting phase were fitted to a model curve, and the resulting bond–slip curve is shown in Fig. 15. Equation (12) was used to calculate the coefficient of determination R^2, which responded to the degree of coupling of the data to the curve, and the results are shown in Table 12. When β was 2.0 in the expression of the slip phase of the bond–slip curve, α was 0.40 in the expression of the cleavage phase, and the R^2 was about 0.90 for the specimens with bar diameters of 14 mm and 16 mm, the theoretical model curve fitted the experimental curves well.

The mean value of R^2 is 0.896, with a standard deviation of 0.028, indicating the robust stability in predictions. Therefore, the segmental expression for the bond–slip curve of reinforced concrete under traveling disturbance is:

$$\begin{cases} \dfrac{\tau}{\tau_{\mathrm{u}}} = \beta\dfrac{s}{s_{\mathrm{u}}} (0 \le s \le s_1) \\ \tau = \tau_{\mathrm{u}}\left(\dfrac{s}{s_{\mathrm{u}}}\right)^{\alpha} (s_1 \le s \le s_2) \end{cases}, \tag{13}$$

where s_1 is the slip corresponding to the progression from the slip phase to the cleavage phase; s_2 is the slip

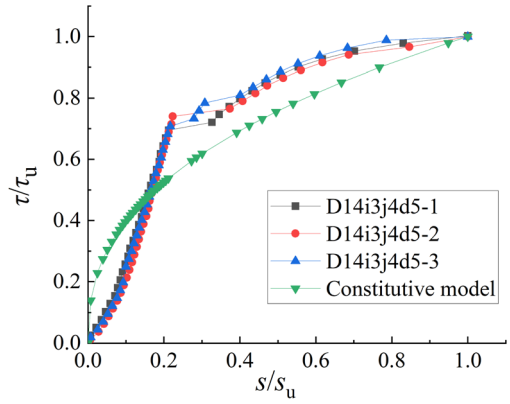

(a) D14i3j4d5

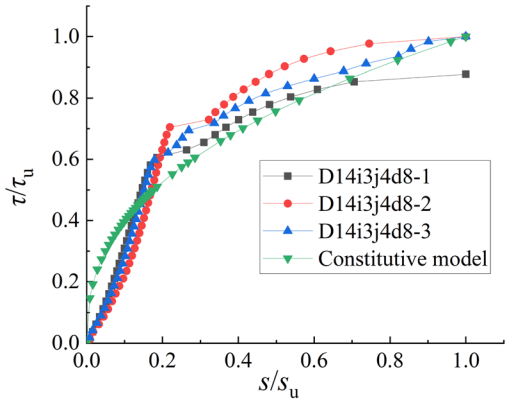

(b) D14i3j4d8

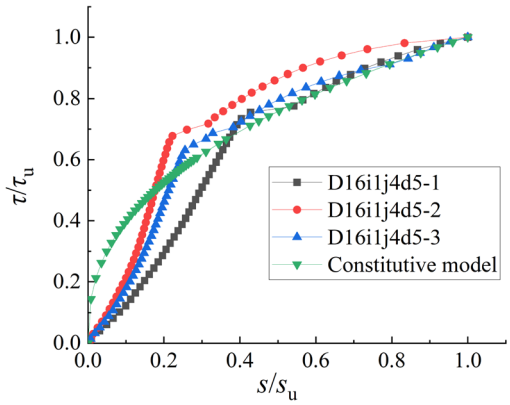

(c) D16i1j4d5

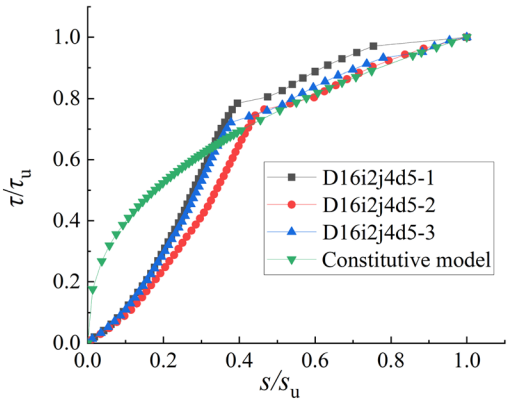

(d) D16i2j4d5

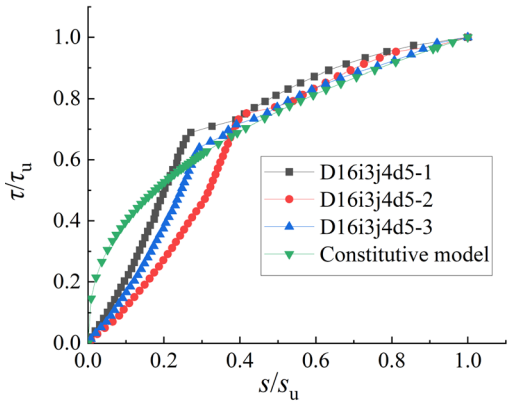

(e) D16i3j4d5

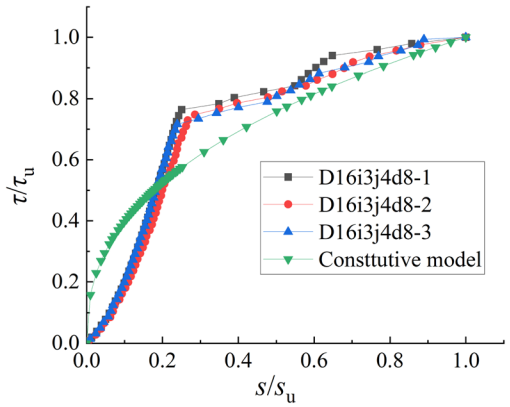

(f) D16i3j4d8

Fig. 14 Comparison of experimental and theoretical bond–slip curves using Eq. (10)

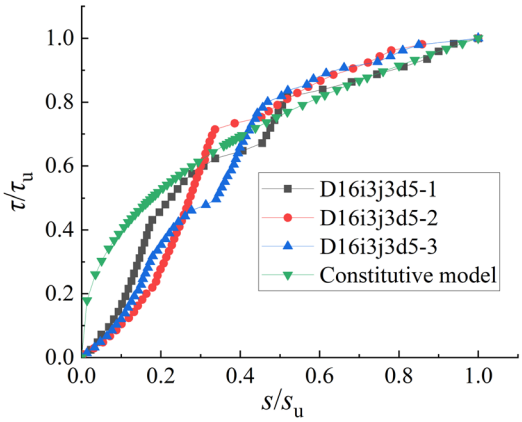

(g) D16i3j3d5

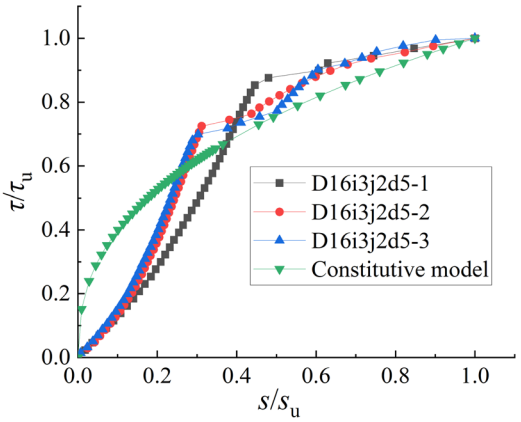

(h) D16i3j2d5

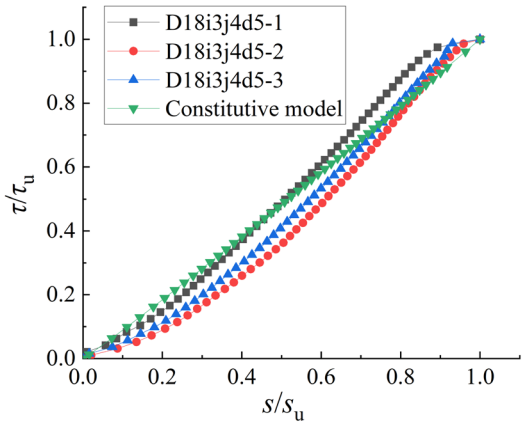

(i) D18i3j4d5

Fig. 14 continued

corresponding to the progression from the cleavage phase to the descent phase. It should be noted that the bond–slip model is applied for the C60 concrete specimens reinforced with HRB400 steel bars.

For the specimens with bar diameters of 14 mm and 16 mm, β was taken as 2.0 for the slip phase of the bond–slip curve, and α was taken as 0.4 for the splitting phase. Equation (13) can be rewritten as:

$$\begin{cases} \dfrac{\tau}{\tau_u} = 2.0\dfrac{s}{s_u} (0 \le s \le s_1) \\ \tau = \tau_u \left(\dfrac{s}{s_u}\right)^{0.4} (s_1 \le s \le s_2) \end{cases} \tag{14}$$

For the specimens with a bar diameter of 18 mm, α or β was taken as 1.0. Equation (13) can be rewritten as:

$$\tau = \tau_u \frac{s}{s_u} \tag{15}$$

5 Conclusions

This study investigates the bond–slip behavior of newly poured concrete and reinforcement bars under traffic-induced vibrations in bridge widening. Center pull-out tests were first conducted on C60 concrete specimens with HTRB400 steel bars. Then, the effects of bar diameter, vibration frequency, amplitude, and anchoring length on the bonding behavior between newly poured concrete and reinforcement bars were analyzed, and practical guidelines for bridge widening were proposed. Finally, the bond–slip constitutive model of newly

Table 10 R^2 of the bond–slip constitutive model fitting curves using Eq. (10)

Specimen no.	α	R^2
D14i3j4d5-1	0.40	0.61
D14i3j4d5-2	0.40	0.63
D14i3j4d5-3	0.40	0.61
D14i3j4d8-1	0.40	0.57
D14i3j4d8-2	0.40	0.62
D14i3j4d8-3	0.40	0.58
D16i1j4d5-1	0.40	0.55
D16i1j4d5-2	0.40	0.54
D16i1j4d5-3	0.40	0.51
D16i2j4d5-1	0.40	0.57
D16i2j4d5-2	0.40	0.62
D16i2j4d5-3	0.40	0.59
D16i3j4d5-1	0.40	0.58
D16i3j4d5-2	0.40	0.65
D16i3j4d5-3	0.40	0.62
D16i3j4d8-1	0.40	0.56
D16i3j4d8-2	0.40	0.62
D16i3j4d8-3	0.40	0.61
D16i3j3d5-1	0.40	0.65
D16i3j3d5-2	0.40	0.59
D16i3j3d5-3	0.40	0.57
D16i3j2d5-1	0.40	0.55
D16i3j2d5-2	0.40	0.65
D16i3j2d5-3	0.40	0.63
D18i3j4d5-1	1.00	0.95
D18i3j4d5-2	1.00	0.92
D18i3j4d5-3	1.00	0.93

poured concrete-reinforcement bars was developed. The primary conclusions are summarized as follows:

(1) A significant increase was observed in the ultimate bond stress of the disturbed specimens. Their failure modes were predominantly characterized by splitting damage. The traffic-induced disturbance enhanced the bonding interaction between the reinforcement and concrete, thereby improving the bond strength of the disturbed specimens.

(2) For the disturbed specimen subjected to a vibration frequency of 4 Hz and a vibration amplitude of 3 mm, the ultimate bond stress decreased as the bar diameter increased. Similarly, the ultimate slip between the reinforced concrete also decreased with an increase in the bar diameter.

(3) As the anchorage length increased, both the ultimate bond stress and the ultimate slip between the reinforced concrete decreased for the disturbed specimens with bar diameters of 14 mm and 16 mm.

Table 11 Linear coefficients β

Specimen no.	τ_u (MPa)	s_u (MPa)	β
D14i3j4d5-1	25.30	1.41	2.17
D14i3j4d5-2	25.47	1.37	2.08
D14i3j4d5-3	25.89	1.43	2.12
D14i3j4d8-1	14.67	1.19	2.28
D14i3j4d8-2	16.42	1.57	2.15
D14i3j4d8-3	16.81	1.54	2.29
D16i1j4d5-1	24.59	1.56	1.97
D16i1j4d5-2	25.65	1.27	2.09
D16i1j4d5-3	26.61	1.54	1.96
D16i2j4d5-1	25.05	1.14	1.87
D16i2j4d5-2	26.07	1.31	1.92
D16i2j4d5-3	24.08	1.23	1.99
D16i3j4d5-1	26.23	1.32	2.08
D16i3j4d5-2	24.80	1.17	1.86
D16i3j4d5-3	24.53	1.24	1.94
D16i3j4d8-1	15.87	1.54	2.04
D16i3j4d8-2	16.42	1.42	1.86
D16i3j4d8-3	16.82	1.60	1.95
D16i3j3d5-1	26.10	1.31	2.13
D16i3j3d5-2	20.74	1.02	1.93
D16i3j3d5-3	27.79	1.30	1.89
D16i3j2d5-1	25.74	1.53	1.83
D16i3j2d5-2	26.87	1.62	1.85
D16i3j2d5-3	21.57	1.05	1.89

(4) The vibration amplitude had a minimal effect on the bond behavior. At vibration frequencies of 2 Hz, 3 Hz, and 4 Hz, the ultimate bond stress between the reinforced concrete decreased as the vibration frequency increased. At the same vibration amplitude, an increase in the vibration frequency caused more damage to the interior of the concrete, leading to a decrease in the bond strength of the specimen.

(5) Based on the experimental data, a bond–slip constitutive model was developed for C60 concrete specimens reinforced with HTRB400 steel bars under traveling

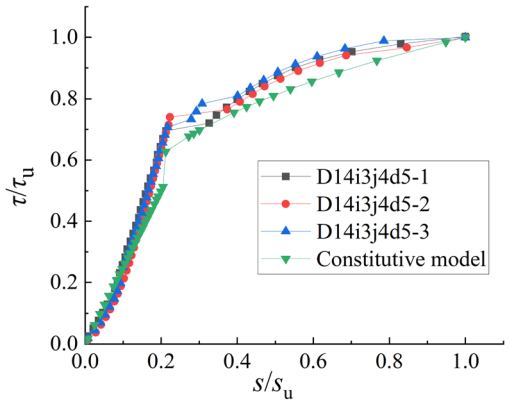

(a) D14i3j4d5

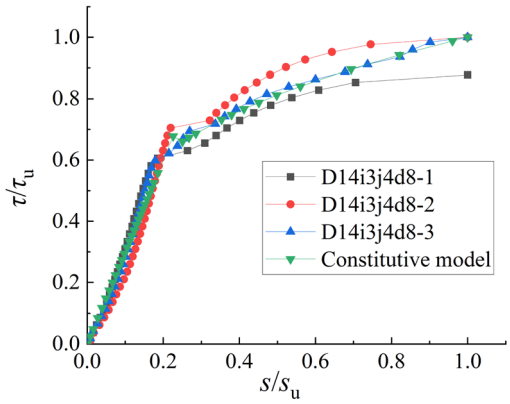

(b) D14i3j4d8

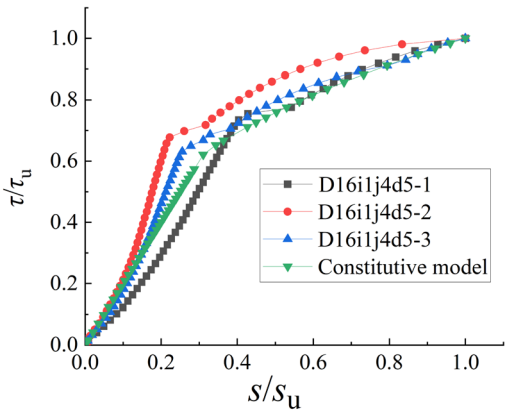

(c) D16i1j4d5

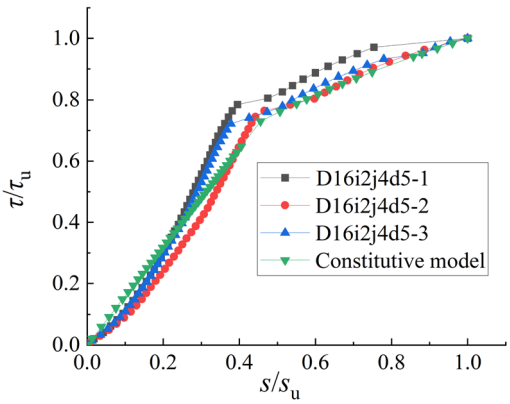

(d) D16i2j4d5

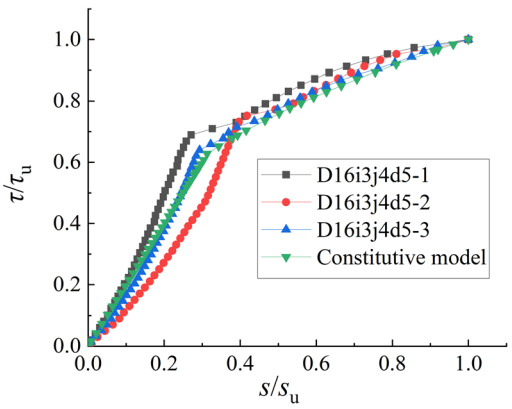

(e) D16i3j4d5

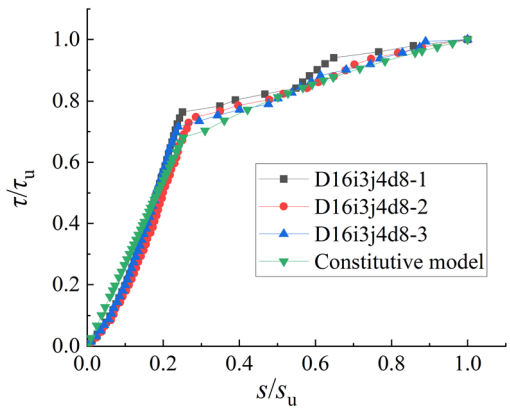

(f) D16i3j4d8

Fig. 15 Segmented bond–slip constitutive model fitting curves

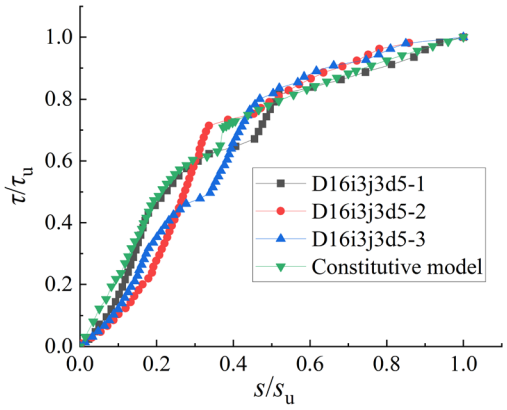

(g) D16i3j3d5

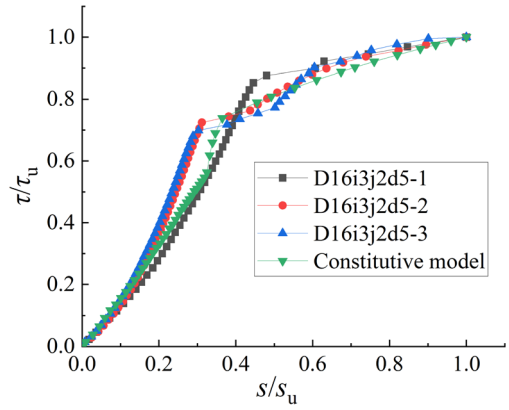

(h) D16i3j2d5

Fig. 15 continued

Table 12 R^2 of the segmented bond–slip constitutive model fitting curves

Specimen no.	B (slip stage)	A (splitting stage)	R^2
D14i3j4d5-1	2.00	0.40	0.89
D14i3j4d5-2	2.00	0.40	0.92
D14i3j4d5-3	2.00	0.40	0.90
D14i3j4d8-1	2.00	0.40	0.91
D14i3j4d8-2	2.00	0.40	0.88
D14i3j4d8-3	2.00	0.40	0.92
D16i1j4d5-1	2.00	0.40	0.87
D16i1j4d5-2	2.00	0.40	0.86
D16i1j4d5-3	2.00	0.40	0.93
D16i2j4d5-1	2.00	0.40	0.89
D16i2j4d5-2	2.00	0.40	0.94
D16i2j4d5-3	2.00	0.40	0.92
D16i3j4d5-1	2.00	0.40	0.86
D16i3j4d5-2	2.00	0.40	0.85
D16i3j4d5-3	2.00	0.40	0.87
D16i3j4d8-1	2.00	0.40	0.90
D16i3j4d8-2	2.00	0.40	0.86
D16i3j4d8-3	2.00	0.40	0.94
D16i3j3d5-1	2.00	0.40	0.91
D16i3j3d5-2	2.00	0.40	0.85
D16i3j3d5-3	2.00	0.40	0.87
D16i3j2d5-1	2.00	0.40	0.92
D16i3j2d5-2	2.00	0.40	0.91
D16i3j2d5-3	2.00	0.40	0.91

disturbance. For specimens with bar diameters of 14 mm and 16 mm, the linear expression coefficient (β) for the slip phase was set to 2.0, and the correction factor (α) for the splitting phase was set to 0.4. For specimens with a bar diameter of 18 mm, both α and β were set to 1.0.

Acknowledgements
This research has been supported by Suqian Sci & Tech Program (Grant No. H202412); the Natural Science Research Project of Jiangsu Province Colleges and Universities (Grant No. 21KJD560002 and Grant No. 23KJA560007), China; Research and Innovation Team Project of Suqian College (Grant No. 2021TD04), China; Suqian Sci & Tech Program (Grant No. H202313), China; Jiangsu Civil Architecture Society project (Grant No. (2023) No. 4 Item 9), China; and the Youth Fund Project of Suqian College (Grant No. 2023XQNA03), China.

Author contributions
Yan Qiao contributed to funding acquisition, conceptualization, formal analysis, investigation, and writing. Weihua Zhang and Jinsheng Cheng contributed to numerical analysis and writing—review. Lei Tong contributed to formal analysis and methodology and supervision. Jibing Deng and Fuhe Gei were involved in formal analysis and methodology. Chuanzhi Sun was involved in validation, project administration, methodology, and writing—review and editing. All the authors read and approved the final manuscript.

Funding
Suqian Sci& Tech Program, H202412, Chuanzhi Sun, Natural Science Research Project of Jiangsu Province Colleges and Universities, 21KJD560002, Chuanzhi Sun, Research and Innovation Team Project of Suqian College, 2021TD04, Chuanzhi Sun, Jiangsu Civil Architecture Society project, (2023) No. 4 Item 9,Chuanzhi Sun, Youth Fund Project of Suqian College, 2023XQNA03, Chuanzhi Sun

Data availability
The data and materials used to support the findings of this study are available from the corresponding author upon request.

Declarations

Ethics approval and consent to participate
Not applicable.

Consent for publication
All the authors agree that the article will be published after acceptance.

Informed consent
Informed consent was obtained from all individual participants included in this study.

Competing interests
The authors declare that they have no competing interests.

Received: 20 October 2024 Accepted: 30 June 2025
Published online: 16 September 2025

References

Charles, K. (1997). Relationships of bond Stress, steel stress, and slip in reinforced concrete. *Journal of Structural Engineering, 6*, 79–85. https://doi.org/10.1061/(ASCE)0733-9445(1997)123:1(79)
Darwin, D., Mccabe, S. L., Idun, E. K., & Schoenekase, S. P. (1992). Development length criteria: Bars not confined by transverse reinforcement. *Structural Journal, 89*(6), 709–720.
Darwin, D., Zuo, J., Tholen, M. L., & Idun, E. K. (1996). Development length criteria for conventional and high relative rib area reinforcing bar. *Structural Journal, 93*(3), 347–359. https://doi.org/10.1021/cen-v074n019.p038
Deng, Y., Li, L., Lv, H., Chen, X., & Ye, Z. (2023). 3D meso-scale numerical model and dynamic mechanical behavior of reinforced concrete. *Structural Concrete, 25*(3), 1819–1839. https://doi.org/10.1002/suco.202300546
Eligehausen R, Popov E P, and Bertero V V. Local bond stress-slip relationships of deformed bars under generalized excitations. Report. No. 83/23, EERC, 1983, University of California, Berkeley, CA.
Feng, X., Li, X., Zhang, C., Liu, X., Li, Y., Gao, S., & Wang, J. (2025). Experimental and numerical study on the bond-slip behavior of high-strength steel bars toward lightweight ultrahigh-performance concrete. *Journal of Building Engineering, 101*, Article 111861. https://doi.org/10.1016/j.jobe.2023.106122
Gao, X. (2003). *Experimental study and numerical simulation of bonding properties of high-performance concrete to reinforcing steel bars*. Tongji University.
Guizani, L., Chaallal, O., & Mousavi, S. S. (2017). Local bond stress-slip model for reinforced concrete joints and anchorages with moderate confinement. *Canadian Journal of Civil Engineering., 44*(3), 201–211. https://doi.org/10.1139/cjce-2015-0333
Haraji, M. H., & Mabsout, M. E. (2002). Evaluation of bond strength of steel reinforcing bars in plain and fiber-reinforced concrete. *ACI Structural Journal, 99*(4), 509–517. https://doi.org/10.14359/12120
Kayyali, O. A., & Yeomans, S. R. (1995). Bond and slip of coated reinforcement in concrete. *Construction and Building Materials, 9*(4), 219–226. https://doi.org/10.1016/0950-0618(95)00024-A
Leroy, A. L. P., & Gergely, P. (1967). Mechanics of bond and slip of deformed bars in concrete. *ACI Journal*. https://doi.org/10.14359/7600
Lin, H., Zhao, Y., Ozbolt, J., Feng, P., Jiang, C., & Eligehausen, R. (2019). Analytical model for the bond stress-slip relationship of deformed bars in normal strength concrete. *Construction and Building Materials, 198*, 570–586. https://doi.org/10.1016/j.conbuildmat.2018.11.258
Lu, C., Ding, P., & Chen, Z. (2011). Time-frequency analysis of acoustic emission signals generated by tension damage in CFRP. *Procedia Engineering, 23*, 210–215. https://doi.org/10.1016/j.proeng.2011.11.2491
Ming, M., Zheng, S., Zhang, Y., Zheng, Y., Yang, S., & Song, M. (2021). Experimental study on the bond-slip behavior and stress transfer mechanism between shaped steel and high-performance fiber-reinforced concrete. *Structures, 34*, 5013–5028. https://doi.org/10.1016/j.istruc.2021.09.014
Mo, Y. L., & Chan, J. (1996). Bond and slip of plain rebars in concrete. *Journal of Materials in Civil Engineering, 8*(4), 208–211. https://doi.org/10.1061/(ASCE)0899-1561(1996)8:4(208)
National standards of People's Republic of China. (2012). *Standard for test method of concrete structures GB/T 50152–2012*. China Standard Press.
Orangun, C. O., Jirsa, J. O., & Breen, J. E. (1977). A reevaluation of test data on development length and splices. *Journal of the American Chemical Society, 74*(3), 114–122. https://doi.org/10.14359/10993
Saeed, M. M., & Houde, J. (1979). Study of Bond Stress slip relationships in reinforced concrete. *ACI Journal*. https://doi.org/10.1016/0022-3115(79)90116-8
Solomos, G., & Berra, M. (2010). Rebar pullout testing under dynamic Hopkinson bar induced impulsive loading. *Materials and Structures, 43*(1–2), 247–260. https://doi.org/10.1617/s11527-009-9485-z
Wu, Y. F., & Zhao, X. M. (2013). Unified bond stress–slip model for reinforced concrete. *Journal of Structural Engineering, 139*(11), 1951–1962. https://doi.org/10.1061/(ASCE)ST.1943-541X.0000747
Xu, T., Bian, X., Liu, Z., Yang, J., & Zhang, Z. (2023). Local bond stress–slip relationship of ribbed reinforcing bars embedded in uhpc: Experiment, modeling, and verification. *Journal of Building Engineering, 68*, Article 106112. https://doi.org/10.1016/j.jobe.2025.111861
Yan C. Bond between reinforcing bars and concrete under impact loading. University of British Columbia, Vancouver, 1992. https://doi.org/10.14288/1.0050492.
Zhou, T., Liu, X., Liu, H., Li, Y., Zhang, P., Chen, H., Chen, Z., Li, L., Shi, J., Kou, J., & Yan, Z. (2022). Experimental study on fire resistance performance of concrete-filled steel plate composite walls. *International Journal of Steel Structures, 23*(2), 389–403. https://doi.org/10.1007/s13296-022-00700-4

Publisher's Note

Yan Qiao is a professor at School of Civil Engineering and Architecture in Suqian College.

Weihua Zhang is an engineer at China Power Engineering Consultant Group Zhongnan Electric Power Design Institute Co. Ltd.

Jinsheng Cheng is an engineer at Suqian City Urban Construction Investment (Group) Co., Ltd.

Lei Tong is an engineer at Suqian City Urban Construction Investment (Group) Co., Ltd.

Chuanzhi Sun is a professor at School of Civil Engineering and Architecture in Suqian College.

Jibing Deng is an engineer at China Construction Fifth Engineering Bureau Co., Ltd.

Fuhe Ge is an engineer at Central Southern China Electric Power Design Institute (CSEPDI) of China Power Engineering Consulting Group Corporation.